# Supporting Information

# Morphology-Phase Coevolution Driven by Oxygen Chemical Potential in $Fe_3O_4$/α-$Fe_2O_3$ Nanosheets

Wenkai Liu[1], Huawei Zhao[1], Dongqi Zhao[1], Yupeng Zhao[1], Muhammad Hamza Tariq[1], Jinhong Du[1], Ruotong Zhao[1], Yanqing Ma[1,2,3,4*] and Lei Ma[1,2*]

[1]Tianjin International Center for Nanoparticles and Nanosystems, Tianjin University, Tianjin, P. R. China, 300072

[2]Tianjin Key Laboratory of Low-dimensional Electronic Materials and Advanced Instrumentation, Tianjin, P. R. China, 300072

[3]Haihe Laboratory for Low-dimensional Electronic Materials, Add 1 to No. 57 Wujiayao street, Hexi District, Tianjin, P. R. China, 300074

[4]School of Precision Instrument and Opto-electronics Engineering, Tianjin University, Tianjin, P. R. China, 300072

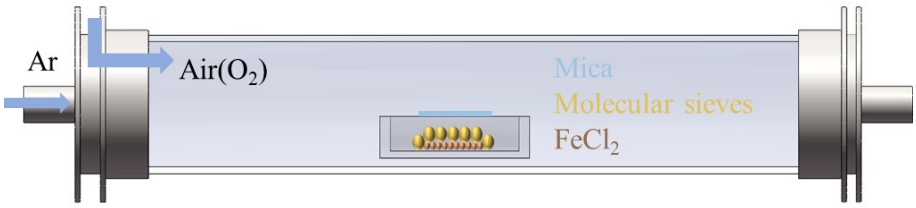


**Figure S1** Schematic illustration of the CVD setup for iron oxide synthesis.

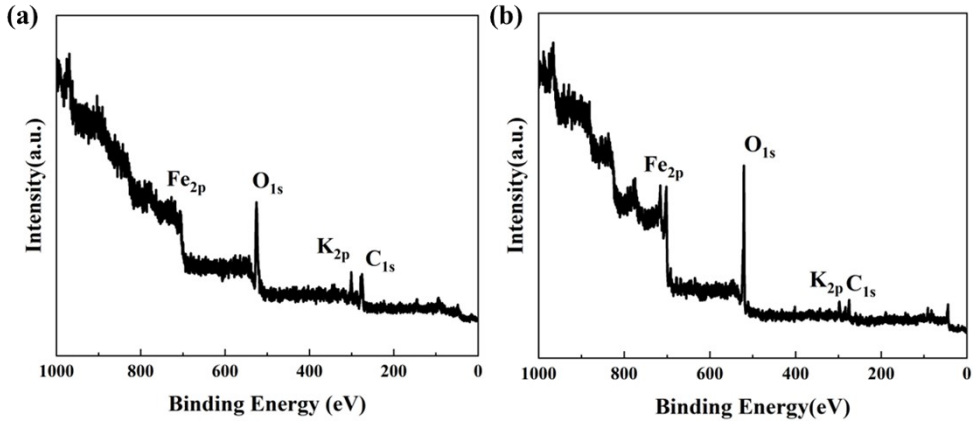


**Figure S2** XPS survey spectra of the synthesized iron oxide phases. **(a)** $Fe_3O_4$ survey spectrum; **(b)** α-$Fe_2O_3$ survey spectrum; the K 2p peak originates from the substrate.

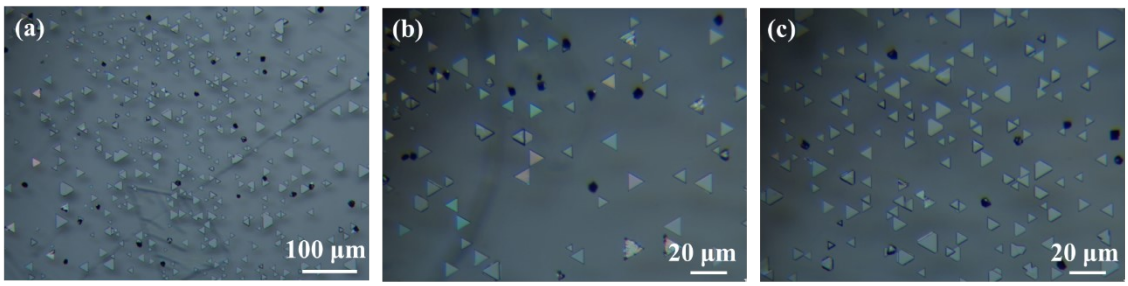


**Figure S3** Optical microscopy images of $Fe_3O_4$ nanosheets from a single synthesis used for shape statistics. Scale bars as indicated.

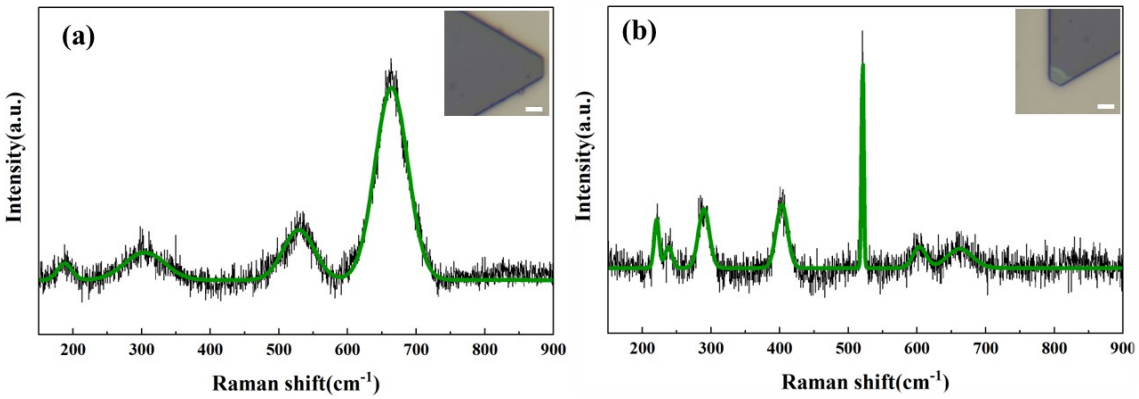


**Figure S4** Raman spectrum indicating the instability of truncated triangular $Fe_3O_4$ nanosheets. **(a)** Raman spectrum with the laser focused at the center; the inset shows no change in the nanosheet after irradiation Scale bars 2 μm; **(b)** Raman spectrum after edge irradiation; the inset shows edge modification induced by the laser.

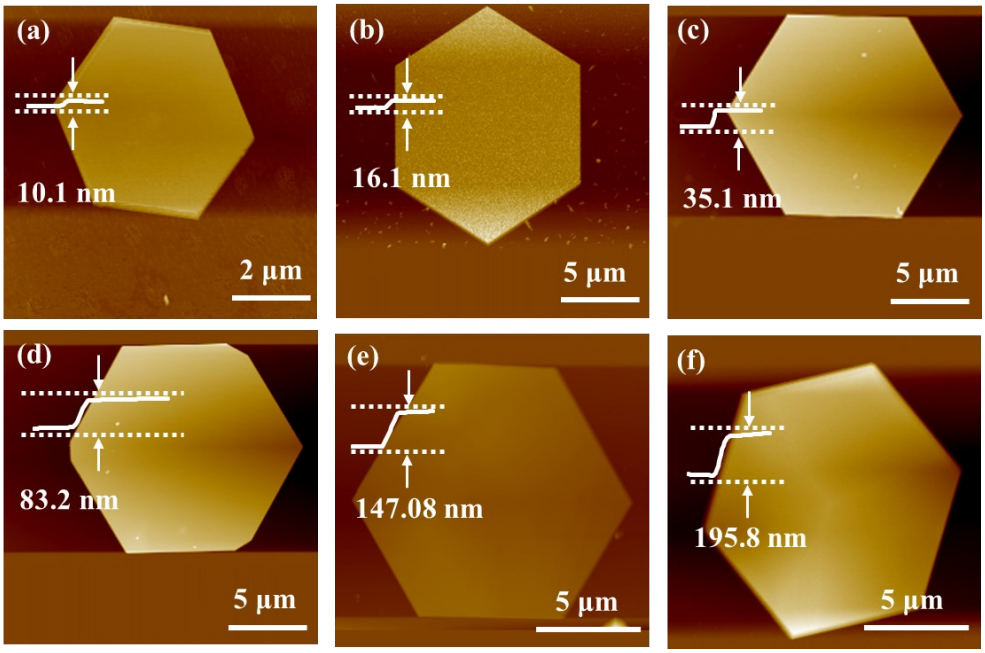


**Figure S5** AFM images of hexagonal α-$Fe_2O_3$ nanosheets of varying thickness synthesized on mica. Scale bars as indicated.

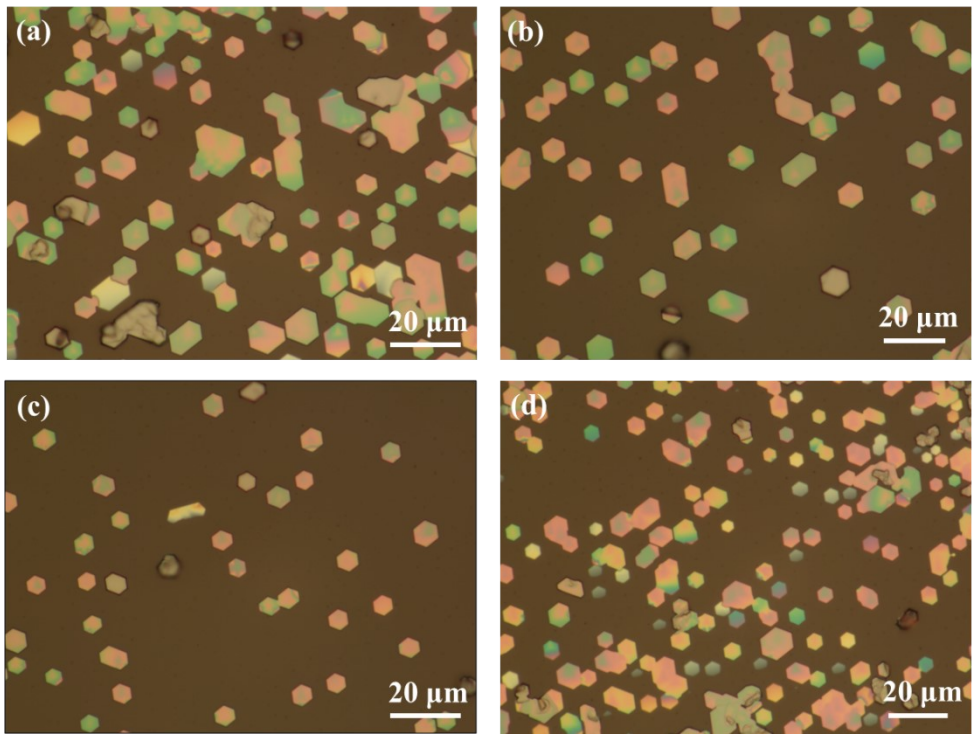


**Figure S6** Optical microscopy images of α-$Fe_2O_3$ nanosheets from a single synthesis used for shape statistics. Scale bars 20 µm.

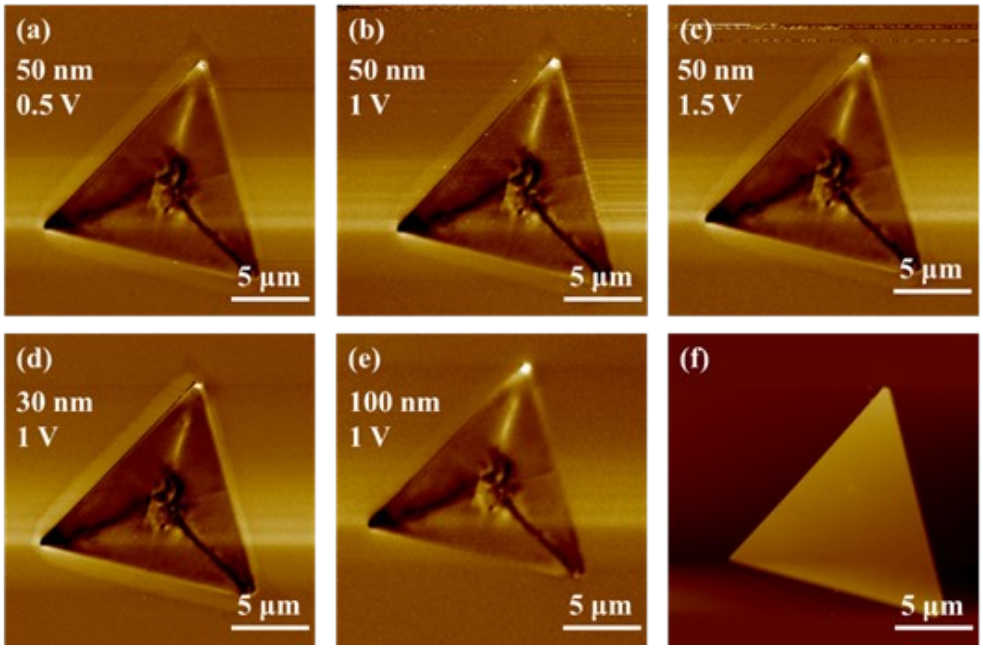


**Figure S7**. In-situ MFM control experiments on a single triangular $Fe_3O_4$ nanosheet. (a-c) MFM images acquired at a fixed lift height of 50 nm with varying drive amplitudes of 0.5 V, 1.0 V, and 1.5 V, respectively. (d-e) MFM images acquired at a fixed drive amplitude of 1.0 V with varying lift heights of 30 nm and 100 nm. (f) Corresponding in-situ NCM topography

image.

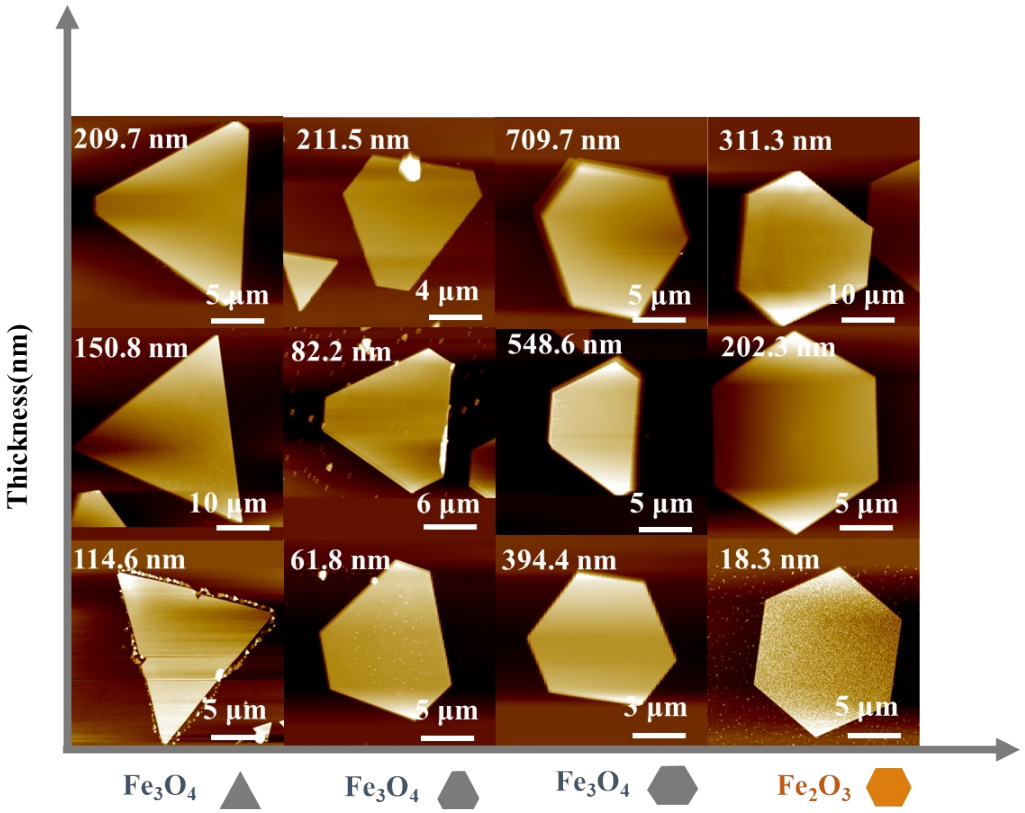


**Figure S8** NCM images of morphology-coupled 2D $Fe_3O_4$ and α-$Fe_2O_3$ corresponding one-to-one to the nanosheets in Figure 4. Scale bars as indicated.

## First-Principles Calculation Details

Surface energies as a function of oxygen chemical potential ($\mu_O$) were computed using VASP 6.4.2 package within the projector-augmented-wave (PAW) formalism and the PBE exchange-correlation functional. All calculations were performed in a spin-polarized framework: α-$Fe_2O_3$ was modeled in its antiferromagnetic ground state, whereas $Fe_3O_4$ was treated as ferrimagnetic, and spin-orbit coupling (SOC) was neglected throughout. A plane-wave cutoff energy of 600 eV was employed, with an electronic self-consistency criterion of $10^{-6}$ eV, and atomic positions were relaxed until the residual forces on all atoms were smaller than 0.02 eV $Å^{-1}$. To properly account for the on-site correlation of Fe 3d and O 2p electrons, the DFT+U approach was adopted, with $U_d$ = 4.0 eV for Fe in $Fe_3O_4$, $U_d$ = 3.81 eV for Fe in α-$Fe_2O_3$, and $U_p$ = 5.90 eV for O 2p states[1].

In the first-principles calculations, Γ-centered Monkhorst-Pack meshes were used for Brillouin-zone sampling. For $Fe_3O_4$ surfaces, 3×3×1, 6×6×1, and 4×3×1 k-point grids were employed for the (111), (001), and (110) terminations, respectively. For α-$Fe_2O_3$ surfaces, 2×2×1, 4×4×1, and 7×2×1 meshes were used for the (110), (001), and (012) terminations, respectively. These choices correspond to a k-point density of approximately, 0.06π $Å^{-1}$, which is sufficient to ensure well-converged total energies and surface energies.

The bulk free energy of $Fe_3O_4$ is approximated as the sum of the free energies of its Fe and O constituents, such that

$$\mu_{Fe_3O_4}^{bulk} = 3\mu_{Fe} + 4\mu_O$$

Under the above assumptions, the surface free energy of $Fe_3O_4$ is given by

$$\gamma = \frac{1}{2A}\left(E_{slab} - E_{bulk}\right) = \frac{1}{2A}[E_{slab} - \frac{1}{3}N_{Fe}\mu_{Fe_3O_4} + \left(\frac{4}{3}N_{Fe} - N_O\right)\mu_O]$$

Where $E_{slab}\ and\ E_{bulk}$are the total energies of the slab and of the bulk reference with the same numbers of atomins, A is the area of one surface of the slab, and $N_{Fe}$ and $N_O$ are the numbers of Fe and O atoms in the slab. The Gibbs free energy expressed as

$$G = E_{el,slab} + E_{vib} + E_{other,intrenal} + PV - TS$$

Where $E_{el,slab}$ is the electronic energy, $E_{vib}$ is the vibrational contribution, $E_{other,intrenal}$ collects other internal-energy terms, and the last two terms are the usual pressure-volume and entropic contributions.

Because the electronic term dominates, we approximate G by $E_{slab}$. For the bulk phase at equilibrium

$$E_{bluk} \approx G = N_{Fe}\mu_{Fe} + N_O\mu_O$$

Where $\mu_{Fe}$ and $\mu_O$ are the chemical potentials of Fe and O, respectively. To relate $\mu_{Fe}$ and $\mu_O$ to the bulk chemical potentials and to define the oxygen-poor limit, we impose the equilibrium constraints

$$\mu_{Fe} \leq \mu_{Fe}^{bulk} \qquad \mu_O \leq \mu_O^{gas}$$

Where $\mu_{Fe}^{bulk}$ is the chemical potential of bulk metallic Fe and $\mu_O^{gas}$ is the chemical potential of oxygen in the gas phase.

# Reference

1. X. Huang, S. K. Ramadugu and S. E. Mason, *The Journal of Physical Chemistry C*, 2016, **120**, 4919-4930.